Contribution of Shape and Gradient Refractive Index to the Spherical Aberration of Isolated Human Lenses

Judith Birkenfeld, Alberto de Castro, and Susana Marcos

Instituto de Óptica "Daza de Valdes," Consejo Superior de Investigaciones Científicas (CSIC), Madrid, Spain

Correspondence: Judith Birkenfeld, Serrano, 121, 28006, Madrid, Spain; j.birkenfeld@io.cfmac.csic.es.

Submitted: February 19, 2014
Accepted: March 20, 2014

Citation: Birkenfeld J, de Castro A, Marcos S. Contribution of shape and gradient refractive index to the spherical aberration of isolated human lenses. *Invest Ophthalmol Vis Sci*. 2014;55:2599–2607. DOI:10.1167/iovs.14-14201

Purpose. To estimate the contribution of 3-dimensional (3D) lens geometry and gradient refractive index (GRIN) to the lens spherical aberration (SA) with age.

Methods. A total of 35 donor human lenses (19–71 years) were imaged with 3D-spectral optical coherence tomography (sOCT). Paraxial and nonparaxial back focal length were measured with laser ray tracing (LRT). The parameters of a 4-variable 3D GRIN model were reconstructed from the data using a global search algorithm. Spherical aberration was calculated for GRIN lenses and their corresponding homogeneous lenses.

Results. Lens thickness and radii of curvature increased significantly with age. Negative anterior conic constant shifted toward more-positive values (slope: 0.228, $P < 0.001$), whereas posterior values remained almost constant (slope: 0.0275, $P = 0.002$). We found a minor decrease and a small significant increase of nucleus and surface refractive index, respectively. The GRIN meridional power exponent had a tendency to increase, indicating a flattening of GRIN distribution, whereas the axial exponent remained almost constant. We did not find a significant age-dependence of the equivalent index. The back focal length had a significant increase with age ($P < 0.001$). The SA shifted toward less-negative values (slope: 0.0249, $P < 0.001$) at higher rates when considering the reconstructed GRIN (slope: 0.041, $P < 0.001$).

Conclusions. Three-dimensional sOCT and LRT allowed reconstruction of lens geometry and GRIN in isolated lenses. The constancy of the GRIN axial power exponent, and the opposite slopes of surface and nucleus indices with age, explain the minor variations of the average index. Both geometrical changes and increase in the GRIN meridional power exponent contribute to the age-dependent shift of negative SA.

Keywords: crystalline lens, spherical aberration, gradient refractive index

The human crystalline lens determines, along with the cornea, the quality of the image projected on the retina. The optical properties of the crystalline lens depend on its geometrical properties and its gradient refractive index distribution.

With age, the human lens undergoes various physical, biometrical, and optical changes.[1] Physical and biometrical changes are well documented as ongoing processes throughout life.[2–9] The lens gets thicker and its surface steeper, and mass and volume increase linearly. Also, the lens gets stiffer with age, which eventually leads to presbyopia, the loss of the capability of the eye to dynamically focus near and far targets.

The geometrical and refractive index changes in the lens result in changes of the optical properties of the eye with age; in particular, the overall spherical aberration (SA) of the eye shifts toward more positive values.[7,10,11] This change in lens SA leads to age-related loss of the corneal/lens SA compensation and a decrease of the optical performance.[12–15]

For unaccommodated eyes in vivo, it was shown that the radius of curvature of the crystalline lens decreases with age.[2,4,8] However, despite this steepening of the relaxed lens, there is no evidence of the eye becoming more powerful with age (a fact known as lens paradox[16]). It has been often postulated that the steepening of the lens is compensated with changes in the equivalent refractive index,[8,17,18] which is supported by experiments that combine phakometric, biometric, and refractive error measurements in vivo.[2,5,6] On the other hand, measurements of isolated lenses in vitro revealed either constant equivalent refractive index with age,[7] or a biphasic behavior with a linear regression up to the breakpoint at age 60.4 years, after which the refractive index remained relatively constant.[19] As isolated lenses in vitro are maximally accommodated,[20] the surfaces of young lenses appeared more curved, and flattened with age, at least until a presbyopic age.[1,19]

Although a potential change of the equivalent refractive index must arise from changes in the distribution of the gradient index, the age-related changes in the refractive index have been most often assessed from comparisons of the estimated power of the eye (from geometrical and biometrical measurements of cornea and lens) and the measured ocular refraction in vivo,[2] or of phakometric and lens power measurements in vitro.[19]

Undoubtedly, a full understanding of the changes in the crystalline lens index with age, and its role in the optical properties of the lens must be obtained from experimental measurements of the gradient refractive index (GRIN). Previous studies report GRIN measurements for various species (fish,[21–23] rat,[24] cat,[25] rabbit,[26] porcine,[27–29] and human[30–34]) using destructive methods[18,34,35] and nondestructive methods, such as ray tracing,[21,24,27,29] magnetic

resonance imaging (MRI),[21,31,32] and optical coherence tomography (OCT).[23,28,30,36]

Measurements of GRIN versus age on human lenses are scarce, and often offer conflicting results. Pierscionek,[34] using a fiber-optic sensor, found that the equatorial edge index, but not the pole index, varied linearly with age. Hemenger et al.,[8] using Purkinje imaging, estimated a flatter profile in the refractive index near the lens center in older lenses than in younger lenses. Jones et al.,[31] using MRI, found a flattening of the refractive index profile in the central region with increasing age, accompanied by a steepening of the profile in the periphery. These results agree with more recent estimations by de Castro et al.,[30] using a 2-dimensional (2D) OCT-based method, which found surface and nucleus refractive indices to be constant with age, but a GRIN profile more distributed in the young lens, and an increase of the central plateau with increasing age.

It has been suggested that GRIN plays a major role in the magnitude of SA of the lens. Jagger[22] proposed that the GRIN distribution balanced the lens' surface SA. Kröger et al.[37] demonstrated the relative contribution of the lens surface and GRIN on SA in fish lenses. In porcine lenses, the estimated SA was predominantly for lenses with a reconstructed GRIN, but positive when considering a homogeneous equivalent refractive index instead; thus, demonstrating a compensation effect by the GRIN distribution.[36]

Similarly, in cynomolgus monkey eyes, the lens SA was negative when calculated using an experimentally estimated GRIN distribution and differed in magnitude from that calculated using a homogeneous equivalent refractive index (for both relaxed and accommodated states).[38]

Although 2D estimates of the GRIN distribution contribute to the comprehension of the role of the GRIN in the optical properties of the lens, 3-dimensional (3D) measurements will allow a full understanding of the interactions between lens shape and internal structures and their relative contribution to the aberrations of the lens, in the young and aging eye.

In the current study, 3D spectral optical coherence tomography (sOCT) measurements on 35 isolated human lenses (between the ages of 19 and 71 years) were used to fully characterize the lens surface geometry and GRIN distribution, using a custom-developed global search algorithm that allowed the reconstruction of the GRIN distribution.[28] The SA was estimated by using computational ray tracing on the lenses with the measured shape and GRIN, and was compared with lenses of equal geometry, but an equivalent homogeneous refractive index. Understanding of the structural changes of the crystalline lens with aging is important to gain insights into the mechanisms of aging of the eye, and in particular presbyopia development and its potential treatment.

Methods

Human Lens Samples and Preparation

Human donor eyes were obtained from Transplant Service Foundation (TSF) Eye Bank. Methods for securing human tissue were in compliance with the Declaration of Helsinki. The handling and experimental protocols had been previously approved by the institutional review boards of TSF and Consejo Superior de Investigaciones Científicas (CSIC). Experiments were performed on 35 eyes from 30 different donors, 1 to 3 days postmortem. The donor age ranged between 19 and 71 years. Presence of cataract was considered an exclusion criterion in the study. All eyes were shipped in sealed vials at 4°C, and wrapped in gauze soaked in preservation medium (DMEM/F-12, HEPES no phenol red; Sigma-Aldrich, St. Louis, MO, USA).

The lens was carefully extracted from the eye and immersed in the same preservation medium at room temperature.[39] During the measurements, the lens was placed on a ring in a DMEM-filled cuvette.

The whole measurement usually took between 1 and 2 hours. Swollen or damaged lenses were identified with the OCT images and excluded from the study.

Optical Coherence Tomography Imaging

All lenses were imaged in 3D using a custom-developed high-resolution sOCT system (described in detail in Grulkowski et al.[40]). The system uses an 840-nm superluminescent diode as illumination source. One 3D image was composed of 1668 A-scans, and 60 B-scans on a 12×12-mm lateral area, acquired in 4.5 seconds. The axial resolution was calculated to 6.9 μm in tissue. The lens axis was aligned with the OCT scan axis such that a specular reflection was seen from the surfaces of the lens. To center and align the lens, real-time display horizontal and vertical A-scans were used.

Images of the lens in 3D were acquired in two different focal planes, to allow visualization of both lens surfaces and the cuvette holding the lens. The images were merged into one complete 3D image of the lens using a custom-developed merging algorithm.[28] Images were obtained with the anterior surface up and with the posterior surface up, after carefully flipping the lens in the holder.

Laser Ray Tracing

The paraxial and nonparaxial focal lengths of each lens were measured using a custom-developed laser ray tracing (LRT) system, which scanned rings of light of different diameters (2 and 4 mm) onto the crystalline lens. The LRT system combined a 2-mirror galvanometric scanning system with a 400-mm collimating lens. The illumination source was a superluminescent diode (849 nm). The crystalline lens was placed in a cuvette (anterior up position) and was aligned with the LRT system, such that the lens and principal ray were collinear to the center of a complementary metal–oxide–semiconductor (CMOS) camera (Thorlabs, Newton, NJ, USA), placed behind the cuvette in the entire focus range. The CMOS captured a series of through-focus images around the focal plane (step size: 0.5 mm).

The system was calibrated using a set of artificial lenses with known back focal lengths, as described in a previous publication.[36] The estimated precision of the focal length measurements was 0.8 mm.

Measurements of the focal length at two different pupil diameters allowed an experimental approximation of the fourth-order Zernike SA, using the following equation[41]:

$$Z_4^0 = \frac{Mr^2}{12\sqrt{5}}, \quad (1)$$

where r is the nonparaxial pupil radius, and M is the difference between optimum powers: $M = M$ (nonparaxial) $- M$ (paraxial). The group refractive index of the solution was taken as $n = 1.345$ at 825 nm.[42]

Image Processing

All OCT images were processed to obtain the shape of the lens surfaces and the surface of the cuvette, using algorithms described in detail in previous publications.[28,36] The distance between surfaces in an OCT image represents the optical path

difference (OPD; geometrical distance multiplied by the refractive index along each A-scan). The anterior surfaces were corrected for fan and optical distortion.[43] The full geometry of the lens was obtained from analysis of the first surface imaged in each condition (anterior surface in "anterior-up" images, posterior surface in "posterior-up" images). All surfaces (lens and cuvette) were fitted by Zernike polynomials (up to seventh order) within a 6-mm pupil. For the purposes of this study, only symmetric Zernike polynomials and astigmatism were used. Additionally, the radii of curvature and conic constant of the surfaces were estimated for 18 meridians using the following equation:

$$z = z_0 - \frac{(x - x_0)^2}{r + \sqrt{r^2 - k(x - x_0)^2}}, \quad (2)$$

where z is the surface sag, x is the radial position along the meridian, r is the apical radius of curvature at the vertex, and k is the conic constant.

The lens thickness was calculated from the distortion of the image of the cuvette surface.[44]

GRIN Reconstruction

The 3D GRIN was reconstructed from lens geometry, OPD, and lens focal length using an updated version of the global search algorithm proposed by de Castro et al.[28] The GRIN was estimated for a 6-mm pupil. The algorithm was run five times for each data set, and was applied in 18 cross-sectional meridians (0–170, in steps of 10°).

Because OCT uses a broadband source, the reconstructed refractive index is the group refractive index at the central OCT beam wavelength (849 nm). It was converted to a phase refractive index at 633 nm to obtain the visible refractive index, using a procedure previously described by Uhlhorn et al.[44] Using the Cauchy equation derived by Atchison and Smith,[45] the group refractive index at 849 nm was converted to its respective phase refractive index, and then to the phase refractive index for visible light.

GRIN Model

The refractive index in the lens is modeled so that it varies continuously from the nucleus to the surface in both axial and meridional directions. The center of the lens is assumed to be in the optical axis at a distance from the anterior surface vertex equal to 0.41 times the lens thickness.[46] The GRIN is described as a four-variable model in polar coordinates:

$$n(\rho, \theta) = n_N - \Delta n \cdot \left(\frac{\rho}{\rho_S}\right)^{p(\theta)}, \quad (3)$$

where n_N is the refractive index of the nucleus, Δn is the difference between the refractive index of surface and nucleus, ρ_S is the distance between nucleus and surface, and $p(\theta)$ is the exponential decay in the axial (p1) and meridional (p2) direction; p1 is constant across meridians, whereas p2 can vary to account for differences between meridians.

Search Algorithm

The GRIN distribution that best fits the experimental data is searched through minimization of a merit function, which is defined by the sum of the root mean square of the differences between the simulated and the experimental OPD from the OCT images and the simulated and experimental focal lengths of the lenses. Because the search involves variables that are strongly coupled, it is probable that a local algorithm would get stuck in local minima. Therefore, a genetic optimization algorithm[47] was implemented as a global search algorithm to prevent the solution falling in a local minimum.[28]

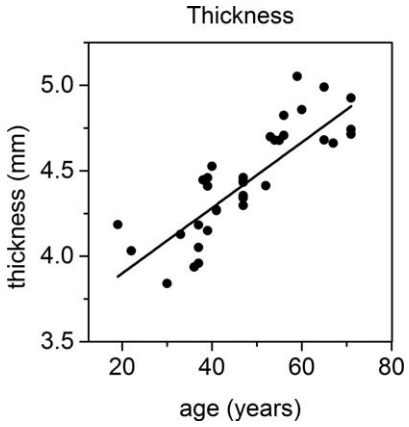

FIGURE 1. Central thickness of isolated human lenses as a function of age, and a linear fit to the data (Thickness [mm] = 0.0196 · Age + 3.5187; $r = 0.84$, $P < 0.001$).

Equivalent Refractive Index and Average Refractive Index

The homogeneous equivalent refractive index was calculated by matching the refractive index producing the same focal length as the lens with the estimated GRIN and using the same 3D geometry. The equivalent index was estimated for a 6-mm pupil diameter.

The average refractive index was calculated directly using the OCT images as the division between the optical thickness and the geometrical thickness.

Computational Ray Tracing Analysis

The optical aberrations of individual lenses were investigated by means of a computational ray tracing analysis using the experimental geometric data of the lens and the reconstructed GRIN. Additionally, aberrations were estimated for the same set of lenses with its equivalent refractive index instead of the GRIN distribution, allowing accounting for the relative contribution of lens geometry and GRIN to the optical properties of the lens.

The custom-developed ray-tracing algorithm is based on the Stavroudis[48] and Sharma et al.[49] algorithm to trace rays through conical surfaces and GRIN, respectively.[28,36] The calculated wave aberrations (fourth-order SA) were fit by Zernike polynomial expansions.

RESULTS

Age Dependence of Crystalline Lens Shape

All lens surfaces were well fitted by conic sections for the central 6 mm of the surface. The root mean square of the residuals of the fittings was below 30 μm. Lens thickness, radii of curvature, and conic constants of the anterior and posterior surfaces were analyzed as a function of age. The thickness increased linearly with age at a rate of 0.0196 mm per year (Fig. 1).

Anterior and posterior radii of curvature (Fig. 2) were fit by a third-order and second-order polynomial, respectively. The anterior lens radii of curvature increased almost linearly up to age 60 (a linear fit between 19 and 60 years showed an increase

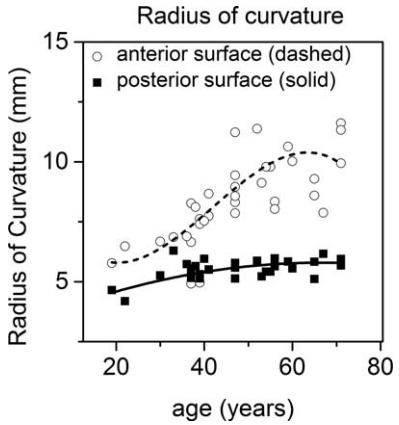

FIGURE 2. Anterior and posterior lens radii of curvature as a function of age. The anterior surface radius was fit by a third-order polynomial (R_{ant}[mm] = $-6E^{-5}x^3 + 0.0082x^2 - 0.2203x + 7.4769$; $r = 0.727$, $P < 0.001$; x = age [years]). The posterior radius of curvature with age was fit by a second order polynomial (R_{pos}[mm] = $-0.0006x2 + 0.073x + 3.5139$; $r = 0.518$, $P = 0.001$; x = age [years]).

of 0.119 mm per year), and tended to decrease beyond that age. Posterior lens radii of curvature tended to increase slightly with age.

Anterior and posterior lens conic constants (Fig. 3) were fit by linear regressions. The anterior surface conic constant was negative for 26 of the 35 lenses (ranging from −16.2 to −0.08), and for all lenses under 47 years. It shifted toward positive values in older lenses, increasing linearly with age at a rate of 0.228 per year ($P < 0.001$). The posterior surface conic constant was −0.17 on average with values between 1.17 and −1.89, and showed a small increase of 0.0275 per year ($P = 0.002$).

Across meridians, the radius of curvature changed by 0.8 mm and 0.32 mm, and the conic constant changed by 2 and 0.12, for anterior and posterior surface, respectively (average values). We did not find any correlation of meridional changes with age. In addition, the magnitude of the changes in the anterior surface was not correlated with those of the posterior surface.

Distribution of the Gradient Refractive Index

The reconstructed parameters for the GRIN are nucleus refractive index (n_N), surface refractive index (n_S), and the power exponents for axial (p1) and meridional (p2) decay.

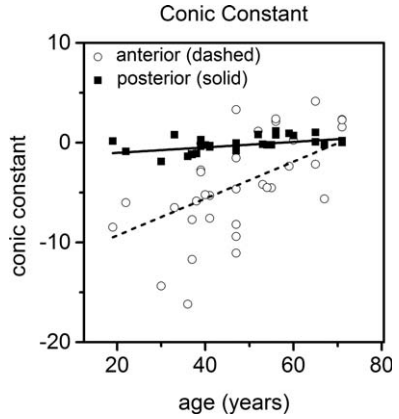

FIGURE 3. Anterior and posterior lens asphericity as a function of age, and linear fit to the data for the anterior lens ($k_{ant} = 0.228 \cdot$ Age $- 14.853$; $r = 0.604$, $P < 0.001$), and for the posterior lens ($k_{pos} = 0.0275x - 1.4798$; $r = 0.5$, $P = 0.002$).

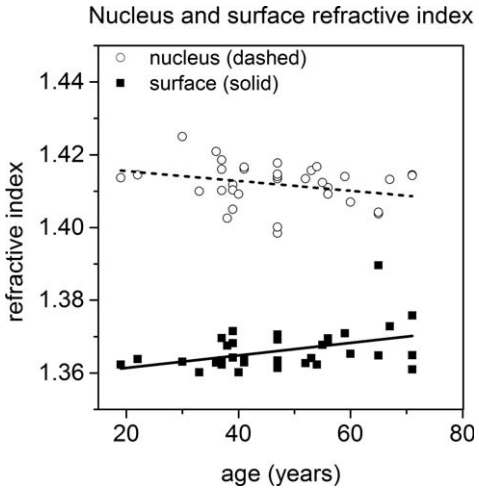

FIGURE 4. Nucleus and surface refractive index as a function of age, and linear fits to the data for the nucleus refractive index ($n_N = -8E^{-5} \cdot$ Age $+ 1.4157$; $r = -0.180$, $P = 0.3$) and the surface refractive index ($n_S = 0.0002 \cdot$ Age $+ 1.358$; $r = 0.409$, $P = 0.015$).

Surface refractive index varied from 1.3601 to 1.3896, and nucleus refractive index between 1.3985 and 1.425 (Fig. 4). The surface refractive index increased by a statistically significant amount with age ($P = 0.015$), at a rate of 0.0002 per year. The nucleus refractive index tended to decrease with age, but its change was not statistically significant ($P = 0.3$).

Figure 5 shows the power exponents in axial (p1) and meridional (p2) directions. The power exponents in the meridional direction (p2) increased ($P = 0.1$), indicating a flattening of the GRIN distribution with age. The power exponent in the axial direction (p1) remained almost constant with age.

The power exponent p2 changed across meridians in some lenses, indicating a contribution of the GRIN to the astigmatism of these lenses. The mean change of p2 was 1.09 with a

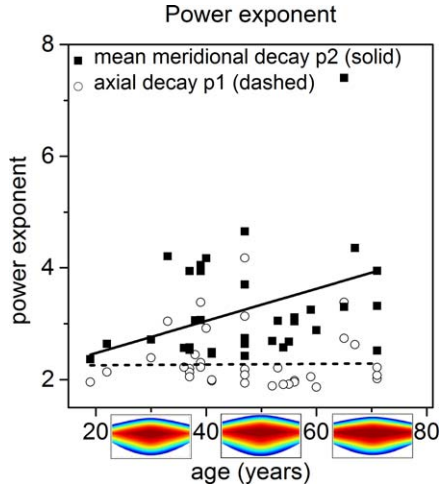

FIGURE 5. Power exponent in the axial direction (p1) and in the meridional direction (p2) as a function of age, and linear fit to the data for p1 (axial decay = $-9.9E^{-4} \cdot$ Age $+ 2.3878$; $r = -0.025$, $P = 0.89$) and p2 (meridional decay = $0.021 \cdot$ Age $+ 2.2973$; $r = 0.281$, $P = 0.1$). For p2, each symbol is the average across 18 meridians. A higher p is consistent with a flatter plateau in the GRIN, and rapid changes toward the surface. The colored insets illustrate a cross section of the GRIN distribution in one meridian. Examples are for lenses of 30, 52, and 71 years.

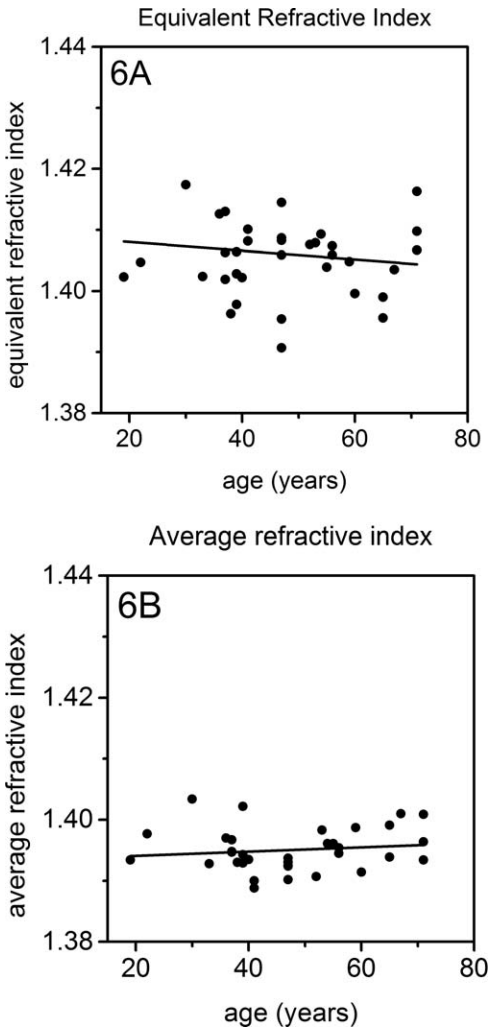

FIGURE 6. (**A**) Equivalent refractive index estimated from the reconstructed GRIN as a function of age, and linear fit to the data (equivalent $RI = -5E^{-8} \pm 0.06 \cdot \text{Age} + 1.405 \pm 3.1$; $r = -0.0001$, $P = 1$). (**B**) Average refractive index, calculated from the OCT images along the optical axis of the lens as a function of age, and linear fit to the data (average $RI = 3E^{-5} \cdot \text{Age} \pm 0.11 + 1.393 \pm 5.4$; $r = 0.14$, $P = 0.44$).

maximum change of 2 in one of the lenses (changes were on average 34%, and always below 58% of the mean value of the meridional exponent).

Equivalent Refractive Index and Average Refractive Index

The equivalent refractive index (Fig. 6A) ranged between 1.391 and 1.417 across lenses, and was 1.406 on average. The average refractive index (along the optical axis, Fig. 6B) ranged between 1.388 and 1.403, and was 1.394 on average. No statistically significant level of correlation was found between age and the refractive indices.

Experimental Back Focal Length

The experimental back focal length (BFL) of the isolated lenses, obtained with LRT, increased significantly ($P < 0.001$) with age, both for a 2-mm (paraxial) and 4-mm (nonparaxial) pupil diameter (Fig. 7). The nonparaxial focal length was relatively higher in younger lenses and changed with age at a lower rate

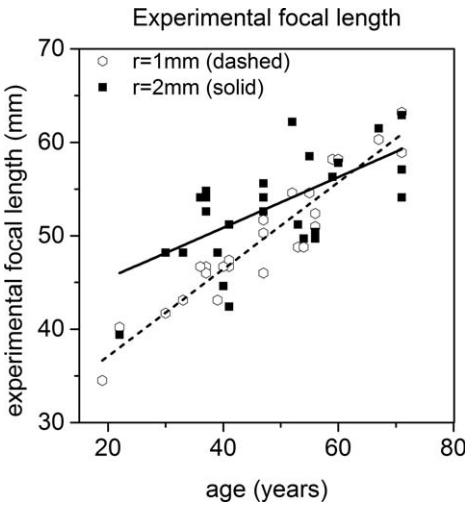

FIGURE 7. Experimental back focal length for a 1-mm pupil radius (paraxial) and a 2-mm pupil radius (nonparaxial), and linear fit to the data for the paraxial ($exp.bfl_{1mm}$ [mm] $= 0.466 \cdot \text{Age} + 27.81$; $r = 0.95$, $P < 0.001$) and nonparaxial data ($exp.bfl_{2mm}$ [mm] $= 0.285 \cdot \text{Age} + 39.070$; $r = 0.66$, $P < 0.001$).

(0.285 mm per year) than the paraxial focal length (0.466 mm per year). Therefore, the difference between paraxial and nonparaxial lens power decreased with age, approaching zero at approximately 63 years of age. The higher central lens power (i.e., a shorter BFL) in the paraxial zone for younger lenses is consistent with negative SA. Therefore, the decrease in the paraxial and nonparaxial BFL difference is consistent with of a shift of SA from negative to more positive values.

Using equation (1), the fourth-order SA Z_0^4 was calculated for the lenses. The SA showed a linear shift with age, from negative values in young lenses to closer to zero in older eyes ($Z_0^4 = 0.0029 \cdot \text{Age} - 0.1904$; $r = 0.455$, $P = 0.022$).

Spherical Aberration: Surface and GRIN Contributions

Figure 8 shows ray-tracing estimates of the lens SA for a 6-mm pupil diameter as a function of age. Calculations were

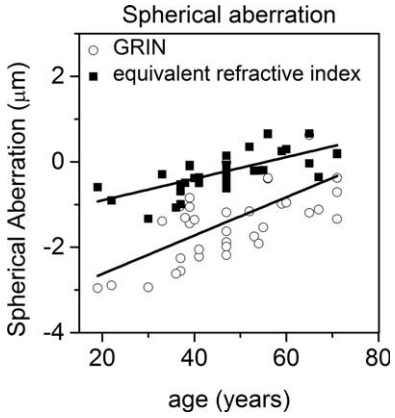

FIGURE 8. Estimated SA as a function of age for GRIN lenses and lenses with a homogeneous refractive index, and linear fits for GRIN lenses (SA_GRIN $= 0.041 \cdot \text{Age} - 3.4075$; $r = 0.654$, $P < 0.001$) and homogeneous refractive index lenses (SA_homogeneous $= 0.0249 \cdot \text{Age} - 1.4043$; $r = 0.696$, $P < 0.001$). The GRIN shifts the SA toward more negative values.

performed for the measured 3D lens geometry and estimated GRIN distribution, as well as for the same lens with a homogeneous equivalent refractive index. The SA shifts significantly toward less-negative values with age, at higher rates when considering the reconstructed GRIN (0.041 per year, $P < 0.001$) than with a homogeneous refractive index (0.0249 per year, $P < 0.001$). The GRIN therefore plays a significant role in the negative values of the crystalline lens SA at all ages, but primarily in young lenses.

Discussion

We have used sOCT to image isolated crystalline lenses of human donors of different ages. These measurements have allowed the quantification of the lens shape and 3D GRIN distribution, and their changes with age. Computational ray tracing on these experimental data allowed evaluating the relative contribution of lens shape and GRIN to SA, as a function of age.

Crystalline Lens Shape Changes With Age

Radius of Curvature. In agreement with previous reports in vitro,[1,19] we found a flattening of the isolated lens (i.e., maximally accommodated) with age. The increase of the radius of curvature was higher (by 45%) in the anterior lens than in the posterior lens (by 20%), between the ages of 20 and 60. Our data also show the biphasic behavior reported by Glasser and Campbell[1] and Borja et al.[19] on isolated crystalline lenses, peaking at approximately 60 years of age. Data are also consistent with measurements in vivo on the fully accommodated state using corrected Scheimpflug imaging,[50,51] Purkinje imaging,[52] and OCT[53] as function of accommodation and/or aging.

In the young lens, the radii of curvature that we report here in vitro are close to those reported in vivo for the maximally accommodated state. Dubbelman et al.[20] reported anterior and posterior lens radii of curvature of 7.0 mm and 5.0 mm, respectively, in a 6D accommodating 25-year-old lens in vivo, in good agreement with the 6.2 mm and 5.0 mm for anterior and posterior radius of an interpolated 25-year-old lens in our study in vitro. Radii of curvature found in vitro are similar in magnitude to those reported in vivo for older lenses by Dubbelman et al.,[20] who reported anterior and posterior lens radii of curvature of 9.5 mm and 5.7 mm, respectively, studying a 60-year-old lens, in agreement with 10.9 mm, and 5.6 mm for a lens of the same age in our study.

Conic Constant. Our data are comparable with the conic constants reported by Dubbelman and van der Heijde[2] for in vivo unaccommodated lenses (−4 to 0.06 for the anterior surface and −3 to 1.96 for the posterior surface), between 16 and 65 years. As expected, the agreement between our in vitro data and in vivo data from Dubbelman et al.[20] is better in older eyes, due to the differences in lens shape between the relaxed accommodation state (in vivo) and the maximally accommodated state (in vitro) in young lenses. In fact, the anterior conic lens constants in the isolated young lenses in our study are in excellent agreement with those reported in maximally accommodated young lenses (−12 to −3, in an age range of 24 to 34 years).[20] In addition, a recent report on accommodating monkey lenses confirm a shift of the anterior conic constant toward negative values with increased accommodation.[38]

The positive anterior lens conic constant in the older eyes is also consistent with results from a study by Manns et al.,[54] who reported an average value of 4.27 in a group of old isolated human lenses (average age 76.4 years).

GRIN Distribution and Equivalent Refractive Index

Age Dependence on Nucleus/Surface Refractive Index. We found a tendency for the nucleus refractive index to decrease with age, and the surface refractive index to increase with age, although only the changes in the surface refractive index showed statistical significance. The range of nucleus and surface refractive index agree with those reported by de Castro et al.[30] using a similar GRIN reconstruction technique, but based on 2D cross-sectional OCT images and a smaller lens sample ($n = 9$), although the relatively high scattering of the values prevented from observing a clear behavior. The higher number of lenses of the current study ($n = 35$) and smaller uncertainties due to the 3D nature of the data allowed us to reach near statistical significance. These data are in agreement with the change in surface refractive index of human lenses (anterior pole only) reported by Pierscionek[34] ($n = 14$), using destructive methods, and the decrease of nucleus refractive index reported by Jones et al.[31] ($n = 20$), using an MRI approach. Also, the decrease of the nucleus refractive index with age is consistent with the hypothesis by Moffat et al.[55] that the lens nucleus experiences an age-related decrease in the soluble protein.

Power Exponent Change. The shape of the GRIN profile changed with age, predominantly in the meridional direction. For some lenses the meridional power exponent p2 changed across meridians, but the magnitude of change was not correlated with age or surface shape (radii, conic constant).

The findings of a more distributed index in younger lenses and an increase of the central plateau with age agree with earlier findings by Hemenger et al.,[8] Moffat et al.,[55] Jones et al.,[31] and de Castro et al.[30] Also, Kasthurirangan et al.[32] reported higher exponents in the equatorial direction than in the axial direction in both young (accommodated) lenses and older lenses, with a larger increase for the equatorial power exponent (from 5.09–10.28) than for the axial power exponent (from 4.04–6.7) with age.

Although the reported power exponent values of the GRIN should better describe those of fully accommodated lenses, as isolated lenses approach a fully accommodated state, we anticipate that the power exponent changes with age in the current study are largely associated with age, and not the accommodation state. This is supported by recent findings by de Castro et al.[38] of the GRIN distribution with simulated accommodation of cynomolgus monkey lenses in vitro, showing no significant differences in the meridional or axial power exponent with accommodation.

It is noticeable that, despite the variability of the results, our estimated power exponents are lower (particularly in older lenses) than earlier reports,[30,32] although they support the increase of the meridional exponent with age. To rule out potential differences associated with the reconstruction model, we repeated the reconstruction using a subset of 2D cross sections from our complete 3D dataset, and a 3-variable model with only one power exponent. In comparison, the power exponent derived from the 2D model showed an age dependence similar to the meridional power exponent derived from the 3D model. This finding suggests that the differences with respect to earlier results obtained from 2D data are likely related to the measured sample, and not to the 2D versus 3D nature of the data. Our power exponent findings reconcile the apparent contradiction in the expression reported by Charman and Atchison in a recent article,[56] where if the power exponent increases (as typically reported to happen with age), then the average refractive index should show a major increase with age. In contrast, another study reports a decrease of the average refractive index with age.[44] Because the average refractive index is dependent only on the axial power

exponent, our finding that axial power exponent is practically constant with age predicts only small differences in the average refractive index with age. Our experimental measurements of average refractive index show a minor increase with age (increase +0.002 from 20- to 70-year-old lenses) in good agreement with the predicted increase (+0.003 in the same age range) by Charman and Atchison.[56] It should be mentioned that our average refractive index results (slightly lower than previous reports) are derived directly from the OCT images (i.e., independent from the GRIN reconstruction).

Equivalent Refractive Index. We found only a small, not statistically significant, decrease of the equivalent refractive index with age. Earlier literature found evidence for a decreasing equivalent refractive index with age in vivo,[2,5,6] but the in vitro results vary.[7,19] Although Pierscionek[34] (isolated lenses) and Glasser and Campbell[1] (isolated lenses) did not find an age dependency of the equivalent refractive index, Borja et al.[19] (isolated lenses) found a significant decrease with age. We expect that this variation is largely associated with age-related changes, and not due to accommodation, and therefore possibly extrapolated in vivo, given the independence of refractive index with accommodation recently reported in monkey lenses.[38,57]

A reason for the discrepancy across data in the equivalent refractive index values in the literature (and its change with age) may be that indirect measurements of the lens power, such as those obtained by comparing lens shape and eye refraction (in vivo) and lens shape and power (in vitro), may be affected by the pupil diameter used (due to the SA of the lens). For example, Dubbelman and van der Heijde[2] calculated the equivalent power from refraction and geometrical data using a 3-mm pupil; Borja et al.[19] calculated the refractive index of crystalline lenses in vitro from the measured equivalent power, thickness, diameter, and radius of curvature, using a 4-mm ring of light as an entrance pupil for the power measurements.

Unlike in previous studies, our equivalent refractive index is obtained directly from our estimated GRIN distribution. In fact, a simulation of the estimation of the equivalent refractive index based on a comparison of the lens power estimated from the lens geometry and GRIN, and the lens geometry and an equivalent refractive index reveals that the estimated equivalent refractive index (and its change with age) is dependent on the pupil diameter used in the calculation. When comparing the results for a 1.5-mm pupil diameter with the results for a 3.0-mm pupil diameter, we found the decrease in the equivalent refractive index to be 35% larger for the smaller pupil diameter. The actual values of the equivalent refractive index changed approximately 1%. Similarly, using the results from the LRT measurements in the estimation, the values for the equivalent refractive index were also higher for smaller pupil diameter (2 mm), and increasing the diameter (to a 4-mm pupil) led to a larger decline (by 20%) with age. Differences in the rate of variation of the equivalent refractive index may therefore be explained by differences in the pupil diameter in the measurements and/or model.

Lens GRIN and Shape Contributions to SA

The SA estimated for the isolated lenses assuming a homogeneous equivalent refractive index was negative in 71.4% of the lenses. When the reconstructed GRIN was assumed instead, the SA was shifted to more negative values, with 97.1% of the lenses showing negative SA .

In both cases, the SA shifted toward less-negative values with age (at rates of 0.025 μm per year for the homogeneous lens and 0.041 μm per year for the GRIN lens). The linear fit crossed zero SA at approximately ages 57 and 84, for homogeneous and GRIN lenses, respectively. Although the compensatory effect of GRIN occurred even in older lenses, this effect decreased significantly with age, and it should be associated with the change in the GRIN distribution (flatter central index).

The negative SA in young human lenses has been reported in numerous studies,[12,14] as well as its shift toward less-negative values with age.[58,59] Furthermore, previous studies have reported a compensatory role of GRIN in different species.[22,28,38,60,61] The current study confirms experimentally the relative contribution of shape and GRIN to SA in human lenses.

It should be noted that the current study exaggerates the negative SA in young lenses, as these are maximally accommodated. With accommodation, the SA shifts toward more-negative values.[53,62] The contribution of lens shape and GRIN to the changes of SA with accommodation has been reported recently in monkey lenses,[38] indicating that GRIN further contributes to the shifts of the SA toward more-negative values with accommodation.

Understanding the role of the crystalline lens structure into the ocular optics is important to understand the factors contributing to optical quality of the eye, its changes with aging, and the development of new IOLs. To our knowledge, this is the first study reporting 3D estimates of human crystalline lens shape and GRIN, and their age dependence, contributing to the understanding of the role and relative importance of the gradient refractive index in the optics of the crystalline lens.

Acknowledgments

Supported by Spanish Government Grant FIS2011-25637 (SM); European Research Council ERC-AdG-294099 (SM); Consejo Superior de Investigaciones Científicas Junta de Ampliación de Estudios (CSIC JAE)-Pre Program (JB); CSIC i-LINK+ 2012, i-LINK+0609 (SM). The research leading to these results has received funding from the European Research Council under the European Union's Seventh Framework Programme (FP7/2007-2013)/ERC Grant Agreement 294099.

Disclosure: **J. Birkenfeld**, None; **A. de Castro**, None; **S. Marcos**, None

References

1. Glasser A, Campbell MC. Biometric, optical and physical changes in the isolated human crystalline lens with age in relation to presbyopia. *Vision Res*. 1999;39:1991–2015.
2. Dubbelman M, van der Heijde RGL. The shape of the aging human lens: curvature, equivalent refractive index and the lens paradox. *Vision Res*. 2001;41:1867–1877.
3. Lowe R, Clark, BR. Radius of curvature of the anterior lens surface. Correlations in normal eyes and in eyes involved with primary angle-closure glaucoma. *Br J Ophthalmol*. 1973;57:471–474.
4. Brown N. The change in lens curvature with age. *Exp Eye Res*. 1974;19:175–183.
5. Garner LF, Smith G. Changes in equivalent and gradient refractive index of the crystalline lens with accommodation. *Optom Vis Sci*. 1997;74:114–119.
6. Atchison DA, Markwell EL, Kasthurirangan S, Pope JM, Smith G, Swann PG. Age-related changes in optical and biometric characteristics of emmetropic eyes. *J Vis*. 2008;8(4):29.1–20.
7. Glasser A, Campbell MC. Presbyopia and the optical changes in the human crystalline lens with age. *Vision Res*. 1998;38:209–229.
8. Hemenger RP, Garner LF, Ooi CS. Change with age of the refractive index gradient of the human ocular lens. *Invest Ophthalmol Vis Sci*. 1995;36:703–707.

9. Koretz JF, Cook CA, Kaufman PL. Aging of the human lens: changes in lens shape at zero-diopter accommodation. *J Opt Soc Am A*. 2001;18:265–272.
10. McLellan JS, Marcos S, Burns SA. Age-related changes in monochromatic wave aberrations of the human eye. *Invest Ophthalmol Vis Sci*. 2001;42:1390–1395.
11. Amano SAY, Yamagami S, Miyai T, Miyata K, Samejima T, Oshika T. Age-related changes in corneal and ocular higher-order wavefront aberrations. *Am J Ophthalmol*. 2004;137: 988–992.
12. Artal P, Guirao A, Berrio E, Williams DR. Compensation of corneal aberrations by the internal optics in the human eye. *J Vis*. 2001;1(1):1–8.
13. Guirao A, Artal P. Corneal wave aberration from video-keratography: accuracy and limitations of the procedure. *J Opt Soc Am A*. 2000;17:955–965.
14. Smith G, Cox MJ, Calver R, Garner LF. The spherical aberration of the crystalline lens of the human eye. *Vision Res*. 2001;41: 235–243.
15. Barbero S, Marcos S, Merayo-Lloves J. Corneal and total optical aberrations in a unilateral aphakic patient. *J Cataract Refract Surg*. 2002;28:1594–1600.
16. Moffat BA, Atchison DA, Pope JM. Explanation of the lens paradox. *Optom Vis Sci*. 2002;79:148–150.
17. Koretz JF, Handelman GH. How the human eye focuses. *Sci Am*. 1988;259:92–99.
18. Pierscionek BK, Augusteyn RC. Species variability in optical parameters of the eye lens. *Clin Exp Optom*. 1993;76:22–25.
19. Borja D, Manns F, Ho A, et al. Optical power of the isolated human crystalline lens. *Invest Ophthalmol Vis Sci*. 2008;49: 2541–2548.
20. Dubbelman M, van der Heijde RGL, Weeber HA. Change in shape of the aging human crystalline lens with accommodation. *Vision Res*. 2005;45:117–132.
21. Garner LF, Smith G, Yao S, Augusteyn RC. Gradient refractive index of the crystalline lens of the Black Oreo Dory (*Allocyttus niger*): comparison of magnetic resonance imaging (MRI) and laser ray-trace methods. *Vision Res*. 2001;41:973–979.
22. Jagger WS. The optics of the spherical fish lens. *Vision Res*. 1992;32:1271–1284.
23. Verma Y, Rao KD, Suresh MK, Patel HS, Gupta PK. Measurement of gradient refractive index profile of crystalline lens of fisheye in vivo using optical coherence tomography. *Appl Phys B*. 2007;87:607–610.
24. Campbell MC. Measurement of refractive index in an intact crystalline lens. *Vision Res*. 1984;24:409–415.
25. Jagger WS. The refractive structure and optical properties of the isolated crystalline lens of the cat. *Vision Res*. 1990;30: 723–738.
26. Nakao S, Fujimoto S, Nagata R, Iwata K. Model of refractive-index distribution in the rabbit crystalline lens. *J Opt Soc Am*. 1968;58:1125–1130.
27. Pierscionek BK, Belaidi A, Bruun HH. Refractive index distribution in the porcine eye lens for 532 nm and 633 nm light. *Eye (Lond)*. 2005;19:375–381.
28. de Castro A, Ortiz S, Gambra E, Siedlecki D, Marcos S. Three-dimensional reconstruction of the crystalline lens gradient index distribution from OCT imaging. *Opt Express*. 2010;18: 21905–21917.
29. Vazquez D, Acosta E, Smith G, Garner L. Tomographic method for measurement of the gradient refractive index of the crystalline lens. II. The rotationally symmetrical lens. *J Opt Soc Am A*. 2006;23:2551–2565.
30. de Castro A, Siedlecki D, Borja D, et al. Age-dependent variation of the gradient index profile in human crystalline lenses. *J Mod Opt*. 2011;58:1781–1787.
31. Jones CE, Atchison DA, Meder R, Pope JM. Refractive index distribution and optical properties of the isolated human lens measured using magnetic resonance imaging (MRI). *Vision Res*. 2005;45:2352–2366.
32. Kasthurirangan S, Markwell EL, Atchison DA, Pope JM. In vivo study of changes in refractive index distribution in the human crystalline lens with age and accommodation. *Invest Ophthalmol Vis Sci*. 2008;49:2531–2540.
33. Pierscionek BK. Surface refractive index of the eye lens determined with an optic fiber sensor. *J Opt Soc Am A*. 1993; 10:1867–1871.
34. Pierscionek BK. Refractive index contours in the human lens. *Exp Eye Res*. 1997;64:887–893.
35. Nakao S, Fujimoto S, Higuchi M, Ito Y. A refractive index distribution of the crystalline lens of the cat eye [in Japanese]. *Nippon Ganka Kiyo*. 1968;19:343–347.
36. Birkenfeld J, de Castro A, Ortiz S, Pascual D, Marcos S. Contribution of the gradient refractive index and shape to the crystalline lens spherical aberration and astigmatism. *Vision Res*. 2013;86:27–34.
37. Kröger RH, Campbell MC, Munger R, Fernald RD. Refractive index distribution and spherical aberration in the crystalline lens of the African cichlid fish *Haplochromis burtoni*. *Vision Res*. 1994;34:1815–1822.
38. de Castro A, Birkenfeld J, Maceo B, et al. Influence of shape and gradient refractive index in the accommodative changes of spherical aberration in nonhuman primate crystalline lenses. *Invest Ophthalmol Vis Sci*. 2013;54:6197–6207.
39. Augusteyn RC, Rosen AM, Borja D, Ziebarth NM, Parel JM. Biometry of primate lenses during immersion in preservation media. *Mol Vis*. 2006;12:740–747.
40. Grulkowski I, Gora M, Szkulmowski M, et al. Anterior segment imaging with spectral OCT system using a high-speed CMOS camera. *Opt Express*. 2009;17:4842–4858.
41. Tarrant J, Roorda A, Wildsoet CF. Determining the accommodative response from wavefront aberrations. *J Vis*. 2010;10(5): 4.
42. Borja D, Siedlecki D, de Castro A, et al. Distortions of the posterior surface in optical coherence tomography images of the isolated crystalline lens: effect of the lens index gradient. *Biomed Opt Express*. 2010;1:1331–1340.
43. Ortiz S, Siedlecki D, Remon L, Marcos S. Optical coherence tomography for quantitative surface topography. *Appl Opt*. 2009;48:6708–6715.
44. Uhlhorn SR, Borja D, Manns F, Parel JM. Refractive index measurement of the isolated crystalline lens using optical coherence tomography. *Vision Res*. 2008;48:2732–2738.
45. Atchison DA, Smith G. Chromatic dispersions of the ocular media of human eyes. *J Opt Soc Am A*. 2005;22:29–37.
46. Rosen AM, Denham DB, Fernandez V, et al. In vitro dimensions and curvatures of human lenses. *Vision Res*. 2006;46:1002–1009.
47. Holland JH. *Adaptation in Natural and Artificial Systems*. Ann Arbor, MI: University of Michigan Press; 1975.
48. Stavroudis OO. *The Optics of Rays, Wavefrons and Caustics*. New York: Academic Press; 1972.
49. Sharma A, Kumar DV, Ghatak AK. Tracing rays through graded-index media: a new method. *Appl Opt*. 1982;21:984–987.
50. Dubbelman M, van der Heijde RGL, Weeber HA. The thickness of the aging human lens obtained from corrected Scheimpflug images. *Optom Vis Sci*. 2001;78:411–416.
51. Koretz JF, Handelman GH, Brown NP. Analysis of human crystalline lens curvature as a function of accommodative state and age. *Vision Res*. 1984;24:1141–1151.
52. Rosales P, Dubbelman M, Marcos S, van der Heijde RGL. Crystalline lens radii of curvature from Purkinje and Scheimpflug imaging. *J Vis*. 2006;6(10):1057–1067.

Investigative Ophthalmology & Visual Science

53. Gambra E, Ortiz S, Perez-Merino P, Gora M, Wojtkowski M, Marcos S. Static and dynamic crystalline lens accommodation evaluated using quantitative 3-D OCT. *Biomed Opt Express*. 2013;4:1595–1609.
54. Manns F, Fernandez V, Zipper S, et al. Radius of curvature and asphericity of the anterior and posterior surface of human cadaver crystalline lenses. *Exp Eye Res*. 2004;78:39–51.
55. Moffat BA, Atchison DA, Pope JM. Age-related changes in refractive index distribution and power of the human lens as measured by magnetic resonance micro-imaging in vitro. *Vision Res*. 2002;42:1683–1693.
56. Charman WN, Atchison DA. Age-dependence of the average and equivalent refractive indices of the crystalline lens. *Biomed Opt Express*. 2014;5:31–39.
57. Maceo BM, Manns F, Borja D, et al. Contribution of the crystalline lens gradient refractive index to the accommodation amplitude in non-human primates: in vitro studies. *J Vis*. 2011;11(13):23.
58. McLellan JS, Marcos S, Prieto PM, Burns SA. Imperfect optics may be the eye's defence against chromatic blur. *Nature*. 2002;417:174–176.
59. Artal P, Berrio E, Guirao A, Piers P. Contribution of the cornea and internal surfaces to the change of ocular aberrations with age. *J Opt Soc Am A*. 2002;19:137–143.
60. Campbell MC, Hughes A. An analytic, gradient index schematic lens and eye for the rat which predicts aberrations for finite pupils. *Vision Res*. 1981;21:1129–1148.
61. Wong K-H, Koopmans SA, Terwee T, Kooijman AC. Changes in spherical aberration after lens refilling with a silicone oil. *Invest Ophthalmol Vis Sci*. 2007;48:1261–1267.
62. He JC, Burns SA, Marcos S. Monochromatic aberrations in the accommodated human eye. *Vision Res*. 2000;40:41–48.

Investigative Ophthalmology & Visual Science